Statistical Validation of a Rocking Numerical Model

Author(s):
Reggiani Manzo, Natalia; Vassiliou, Michalis F.; Mouzakis, Harris; Badogiannis, Efstratios

Publication date:
2022

Permanent link:
https://doi.org/10.3929/ethz-b-000571382

Funding acknowledgement:
ETH-10 18-1 - Seismic analysis, design and experimental testing of precast controlled-rocking negative-stiffness systems (ETHZ)

Statistical Validation of a Rocking Numerical Model

Natalia Reggiani Manzo – ETH Zurich, Zurich, Switzerland, e-mail: reggianimanzo@ibk.baug.ethz.ch

Michalis F. Vassiliou – ETH Zurich, Zurich, Switzerland, e-mail: vassiliou@ibk.baug.ethz.ch

Harris Mouzakis – National Technical University of Athens, Athens, Greece, e-mail: harrismo@central.ntua.gr

Efstratios Badogiannis – National Technical University of Athens, Athens, Greece, e-mail: badstrat@central.ntua.gr

Abstract: Validation of numerical models is a paramount task for the design of structures and introduction of new construction solutions in practice. Up to now, rocking structures have been considered unpredictable, hampering their use in practice. Using a recently proposed statistical validation method, this paper claims that rocking motion can be predicted. Herein, a simple 3D wobbling rocking model is statistically validated against multiple shake table tests. Both numerical and experimental seismic response are clustered in six bins, sorted according the excitation type and intensity, and their cumulative distribution functions and median response are compared. The paper shows that, even though the numerical model does not account for sliding and twisting of the columns, it still represents well the statistics of the horizontal displacement of the rocking system. Only in 1 out of the 6 cases the numerical model fails to predict well the statistics of the tested rocking system. Thus, as structures are usually designed for set ground of motions and not individual ground motions, the paper claims that the statistical validation is sufficient and appropriate for validation of rocking models.

Keywords: model validation, uplifting structures, precast structures, response prediction

1. Introduction

In the recent years, rocking has been proposed as a resilient alternative for precast bridges in seismic active regions. Mander and Cheng (1997), Palermo et al. (2004), Cohagen et al. (2008), Mashal (2015), Sideris et al. (2015), Thonstad (2016), Qu et al. (2018), Salehi et al. (2021) have suggested to construct prefabricated rocking bridges by connecting precast elements via ungrouted post-tensioned tendons, forming dry connections. The dry connection allows the elements to rock, avoiding the formation of plastic hinges, while the elongation of the tendon is distributed along all its length, preventing yielding of the reinforcement. Hence, the tendon offers a recentering mechanism and the structure does not present damage.

Depending on the tendon's axial stiffness, the proposed system may present positive or negative lateral stiffness (Vassiliou & Makris, 2015; Makris & Vassiliou, 2015). Focusing on the performance of the superstructure and the easy relation of the system's seismic response to available design spectra, rocking systems with positive stiffness have been more extensively explored (Kurama et al., 2018; Zhang & Alam, 2020; and references therein). Systems with lateral negative stiffness, however, can potentially reduce the design moments on the foundation, and consequently, its size. The reinforced concrete used for the foundation can sometimes comprise up to 50% of the total amount used in the project. Therefore, the reduction of forces transmitted to the foundation leads not only to a resilient alternative for precast bridges, but also to a more sustainable design alternative, as it can reduce the foundation size and save material.

Despite its potential benefits, the response of rocking systems with negative lateral stiffness is highly nonlinear (Makris & Konstantinidis, 2003). Any small changes on the initial and boundary conditions of the problem leads to significantly different responses. Thus, it has been claimed that the rocking motion is unpredictable and numerical models could not be validated. Bachmann et al. (2018) and Vassiliou et al. (2021) have shown that numerical models used to describe rocking systems can be validated through methods that statistically compare the numerical and experimental response to sets of ground motions. This a weaker but sufficient validation method.

In an attempt to further develop seismic design of systems with negative stiffness, this paper statistically validates the wobbling model proposed by Vassiliou (2018) and Vassiliou et al. (2017). The experimental dataset originates from the results of the experimental campaign conducted at the National Technical University of Athens (NTUA) in collaboration with ETH Zurich, which consisted of multiple shaking table tests of a slab supported on four precast columns. The slab was connected to the columns only through the ungrouted tendons in series with washer springs, and the whole system was simply standing on top of the shake table platform.

2. Mechanics of the rocking frame

2.1. Static planar behavior

Fig. 1a presents a rocking frame comprising N rigid columns of total mass $N \times m_c$ and a rigid beam of mass m_b. The columns are able to uplift but not slide at any end. They are restrained with a perfectly elastic restraining system, composed of tendons anchored at the bottom end of the columns and the above the beam, in series with a spring. The total stiffness of the restraining system (i.e., spring + tendon) is k_{res}.

Assuming a horizontal force F applied at the beam, the linearized lateral force–deformation relation ("pushover curve") is:

$$F = \left(\frac{1}{2}+\gamma\right) N m_c g \,\mathrm{sgn}(u) + \left(\frac{N k_{res} b\alpha}{2} - \left(\frac{1}{2}+\gamma\right) N m_c g\right)\frac{u}{2h} \qquad (1)$$

Fig. 1b plots Equation 1 for different values of k_{res}. For all values of k_{res}, the system presents a bilinear elastic behavior. There is no hysteresis and unloading follows the same branch. When $k_{res} = 0$ (i.e., no tendon), the post-uplift stiffness of the system is negative. Collapse is reached not because of material failure, but when the restoring force becomes zero, that is, when the columns reach the point of neutral equilibrium. This defines the displacement capacity of the system.

Adding a non-prestressed tendon algebraically increases the post-uplift stiffness. When the stiffness remains below $k_{crit} = \dfrac{(1+2\gamma)\, m_c g}{b\alpha}$, the post-uplift stiffness of the system remains negative, the slope of the second branch is milder, and the displacement capacity increases (Vassiliou & Makris, 2015; Makris & Vassiliou, 2015). Reggiani Manzo & Vassiliou, (2022a) have validated the above equations through cyclic tests.

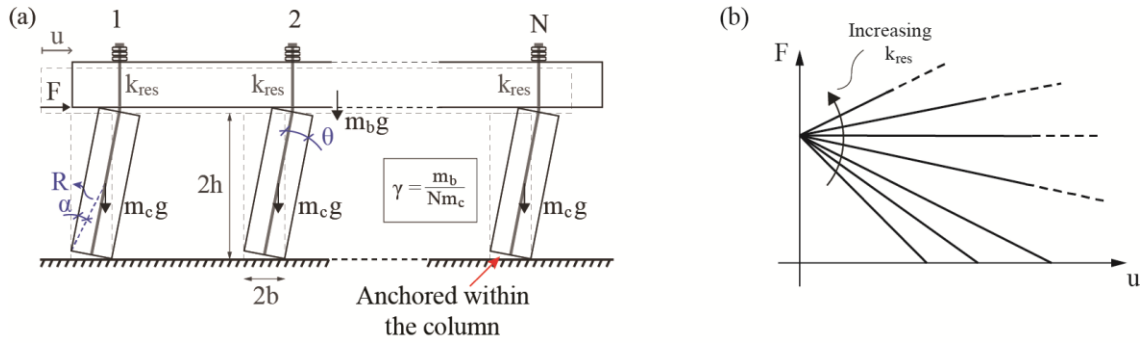

Fig. 1 – (a) Rocking frame with vertical restrainers, and (b) its force-deformation relationship.

2.2. Dynamics of the planar rocking frame

Based on Makris & Vassiliou (2015), and assuming that the columns are always in contact with the ground, the linearized equation of motion of the restrained rocking frame (Fig.1a) is:

$$\ddot{u} + \frac{1+2\gamma}{1+3\gamma}\frac{3g}{2}\alpha\,\mathrm{sgn}(u) + \left(\frac{3}{2}\frac{1}{1+3\gamma}\frac{\alpha k_{res} b}{m_c} - \frac{3g}{2}\frac{1+2\gamma}{1+3\gamma}\right)\frac{u}{2h} = -\frac{3}{2}\frac{1+2\gamma}{1+3\gamma}\ddot{u}_g \qquad (2)$$

Unless extra yielding or friction dissipation device is provided, energy is only dissipated during impact, and it is usually taken into account via a coefficient of restitution (Housner, 1963) defined as the ratio between the columns' angular velocity after ($\dot{\theta}_{\text{after}}$) and before ($\dot{\theta}_{\text{before}}$) the impact:

$$r = \frac{\dot{\theta}_{\text{after}}}{\dot{\theta}_{\text{before}}} \qquad (3)$$

2.3. Three-dimensional model

Fig.2 shows a 3D extension of the rocking frame model (Vassiliou, 2018; Vassiliou et al., 2017). The assumptions of the planar frame (i.e. rigid body, no sliding or "flying", and pointwise contact) are extended to include the following:

- The columns are constrained to not roll-out of its initial position.
- The columns are always in contact with the support and the slab. Therefore, the contact forces are always compressive.
- No damping mechanism is included.

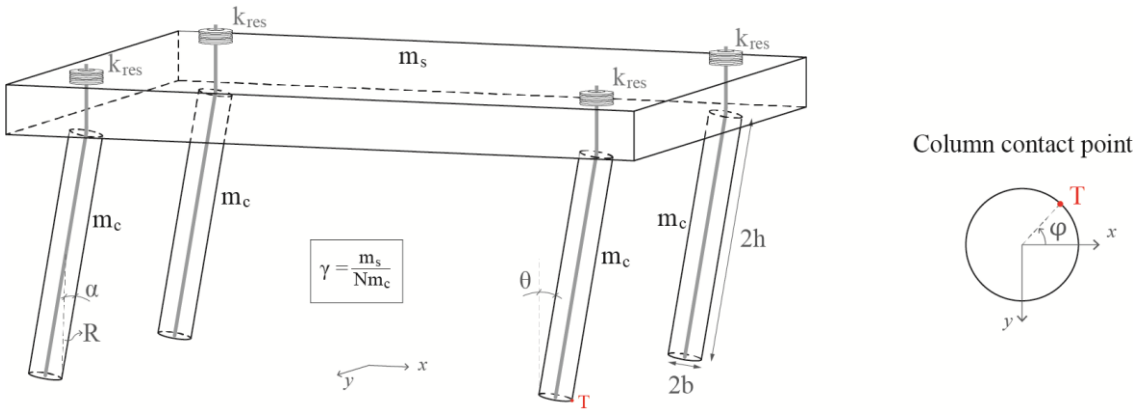

Fig.2 – Three-dimensional wobbling frame.

- The tendon is anchored above the spring and within the column.

Then, the equations of motion become:

$$\ddot{\theta} = -\hat{p}^2 \left(\begin{array}{l} \sin(\alpha-\theta) + \cos(\alpha-\theta)\left(\frac{\ddot{u}_g}{g}\cos\varphi + \frac{\ddot{v}_g}{g}\sin\varphi \right) \\ + \frac{k_{res}\cdot 2h}{m_c g}\frac{1}{2(2\gamma+1)}\sin\alpha\tan\alpha\sin\theta \end{array} \right)$$
$$+\dot{\varphi}^2 \left(\begin{array}{l} \sin\theta\sin^2\alpha\left(4\gamma+\frac{3}{2}\right) + \cos\alpha\sin\alpha(4\gamma+1)(1+\cos\theta-2\cos^2\theta) \\ +\sin\theta\cos\theta\left(\frac{4}{3}\cos^2\alpha - \frac{5}{4}\sin^2\alpha + 4\gamma(\cos^2\alpha-\sin^2\alpha)\right) \end{array} \right) \frac{12}{48\gamma+15+\cos^2\alpha} \quad (4)$$

$$\left(\begin{array}{l} \left(\frac{4}{3}\cos^2\alpha - \frac{5}{4}\sin^2\alpha + 4\gamma(\cos^2\alpha-\sin^2\alpha)\right)\sin^2\theta \\ +(3+8\gamma)(1-\cos\theta)\sin^2\alpha + 2\sin\alpha\cos\alpha\sin\theta(1+4\gamma)(1-\cos\theta) \end{array} \right) \ddot{\varphi}$$
$$+ \left(\begin{array}{l} (3+8\gamma)\sin^2\alpha\sin\theta + \left(\frac{8}{3}\cos^2\alpha - \frac{5}{2}\sin^2\alpha + 8\gamma(\cos^2\alpha-\sin^2\alpha)\right)\sin\theta\cos\theta \\ +2\cos\alpha\sin\alpha(1+4\gamma)(2\sin^2\theta+\cos\theta-1) \end{array} \right) \dot{\varphi}\cdot\dot{\theta} \quad (5)$$
$$= (2\gamma+1)\left(\sin\alpha + \sin(\theta-\alpha)\right)\frac{\ddot{u}_g\sin\varphi - \ddot{v}_g\cos\varphi}{R}$$

where

$$\hat{p}^2 = \frac{12(2\gamma+1)}{48\gamma+15+\cos^2\alpha}\frac{g}{R} \quad (6)$$

θ is the tilt angle, φ is the angle defining the contact point, T, between the column and the support (Fig. 2).

3. Shake table testing

In order to statistically validate the numerical model presented in Section 2.3, a series of tests was performed at the Laboratory for Earthquake Engineering (LEE) of the National Technical University of Athens (NTUA).

3.1. Specimen

For the sake of brevity, this paper discusses only briefly the design and detailing of the specimen. All information about the design, detailing and construction of the specimen can be found in Reggiani Manzo et al. (2022b, 2022c).

The tested specimen, shown in Fig. 3, consisted of four reinforced concrete columns supporting a reinforced concrete slab. The columns were freely standing on the shake table platform, and connected to the slab only via unbonded non-prestressed restraining tendons in series with 10 washer springs. The combination of washer springs and the tendon was necessary to obtain a restraining system flexible enough to keep the rocking frame's lateral stiffness negative. At the displacement capacity of the specimen, it was estimated that the final secant stiffness of the restraining system was 1720 kN/m.

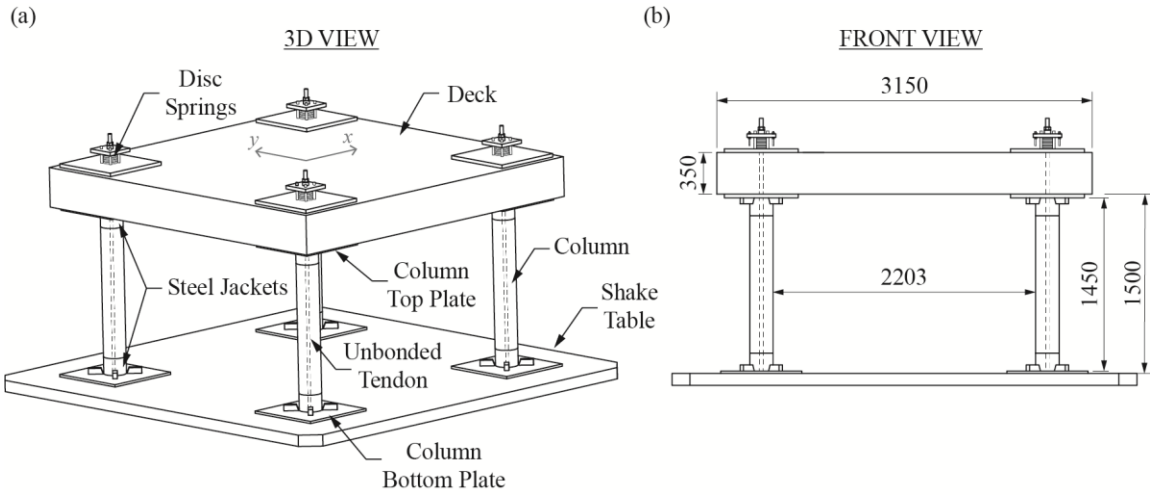

Fig. 3 – Schematic drawing of the specimen in (a) 3D View, and (b) Front View.

To avoid damage to the ends of the column due to stress concentrations and impact, the columns ends were confined by steel jackets. Furthermore, steel plates were also placed in the interface of the column with the slab and the shake table. The plates were equipped with restrainers that limited sliding to 5 mm in each direction.

The specimen was designed with a redundant mechanism to prevent toppling of the columns, while protecting the tendons from exceeding their yield capacity. The redundant mechanism consisted of two threaded rods placed in parallel with each stack of washer springs, which would engage only after a 15-mm deformation of the stack of springs. To protect the tendons, which could not be easily replaced without disassembling the specimen, the threaded rods were designed as sacrificial elements, yielding at a smaller load than the tendons.

Even though the tested specimen was not designed to represent a specific prototype bridge, a 1:5 scale was assumed. At prototype scale, this scaling factor would lead to 7.25 m-high columns, which falls within the range of typical heights of columns of highway bridges, although on the lower end. The column aspect ratio (height to width) was slightly larger than typical highway bridges.

3.2. Shaking table specifications

The tests were performed in the 4 × 4-m six degree-of-freedom shaking table of NTUA. The maximum stroke and velocity of the simulator in the three axes are ±100 mm and 1000 mm/s, respectively. Under 10 tons of payload, the maximum acceleration of the horizontal axes is 2g, while a 4g acceleration is permitted in the vertical direction.

3.3. Excitation selection and scaling

The specimen was subjected to all three sets of ground motions proposed by FEMA P695 (2009) (near-field pulselike (NFP), near-field no pulse-like (NF), and far-field (FF)). The sets are composed of 14 NFP, 14 NF, and 22 FF ground motions. In addition to the ground motions proposed by FEMA, an extra 12 NFP, 12 NF, and 21 FF ground motions were included. Moreover, the original FF set of ground motions proposed by FEMA includes Cape Mendocino, Rio Dell Overpass record. However, this was not available in the PEER ground motion database and, thus, was not included in this study.

In total, this experimental campaign consisted of 26 NFP, 26 NF, and 42 FF ground motions. The details of the records, along with the adopted numbering scheme, are provided in Reggiani Manzo et al. (2022b, 2022c).

All sets of ground motions were scaled to the same $\overline{\text{PGV}}$, which was defined herein as:

$$\overline{\text{PGV}} = \sqrt{\left(\text{PGV}_x\right)^2 + \left(\text{PGV}_y\right)^2} \quad (7)$$

where PGV_x and PGV_y are the peak ground velocities along the *x* and *y* directions.

Respecting the capacity of the shake table, two different $\overline{\text{PGV}}$ levels were selected (in the model scale): (a) low $\overline{\text{PGV}}$ = 16.75 cm/s and (b) a high $\overline{\text{PGV}}$ = 33.5 cm/s. Overall, there were three different ground motion sets (NFP, NF, and FF) scaled at two different $\overline{\text{PGV}}$, which resulted in 188 ground motions. The longitudinal, lateral, and vertical components of each ground motion were simulated by the shake table.

As a length scale of 1:5 was assumed for the column height, to preserve similitude of time, the excitations were scaled in time to $S_T = \sqrt{S_L}$, in which S_L is the length scale equal to 1/5. In the prototype scale, this corresponds to a $\overline{\text{PGV}}$ of 37.5 and 75 cm/s at the low- and high-intensity sets, respectively.

The order of the tests was defined based on the system's response predicted using the analytical model proposed by Vassiliou (2018). The excitations were sorted from the smallest to largest predicted displacement. Some ground motions could not be simulated either because the structure failed before its execution or because the shake table could not reproduce them sufficiently accurately. The test order is also provided by Reggiani Manzo et al. (2022b, 2022c).

3.4. Instrumentation

Fig.4 presents the location of all instruments installed on the specimen. The horizontal displacements of the slab were measured using draw-wire sensors, the vertical displacements using cable-extension position transducers, and the accelerations using accelerometers. Load cells were also installed in series with the tendons of each column. The deformation of the spring system of column C2 was recorded using string potentiometers. Furthermore, the sensors integrated into the actuators of the shaking table recorded the displacement and acceleration of the table platform.

4. Experimental observations

As the goal of this paper is to statistically validate the numerical model for restrained rocking bridges previously presented, the experimental observations are only briefly presented herein. The observed seismic behavior of the tested specimen is extensively discussed in Reggiani Manzo et al. (2022b).

During the execution of the tests, it was observed that the columns twist and slide relatively to the shake table and the slab. Nonetheless, with exception to the excitation that caused the unexpected collapse of the specimen, the sliding restrainers were sufficient to restrain the sliding of the columns.

The system eventually collapsed when it was excited by the ground motion 1987, Superstition Hills-02 scaled to the high-intensity set. The collapse was caused by the unexpected failure of the tendon of column C1 that was followed by the failure of tendon

of column C2. The collapse was unexpected because the tendons failed prematurely: C1 broke at 98.8 kN and C2 at 105.4 kN, while the yielding load specified by the tendon's manufacturer was 237 kN. Both tendons failed at their sockets, indicating some unexpected stress concentration during the manufacturing process.

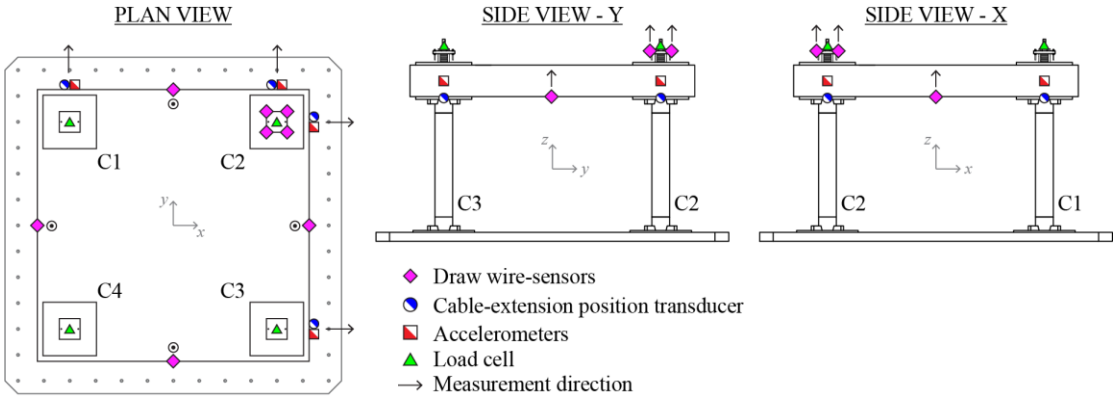

Fig. 4 – Instrumentation location.

The specimen was visually inspected after each excitation and after the collapse. No cracks and concrete spalling could be observed in the columns and steel jacket. The only observed damage was abrasion of the edges of the top and bottom steel jacket, being the abrasion of the top steel jackets more pronounced.

5. Statistical Validation

This section statistically validates the model presented in Section 2.3 by comparing its predictions to the shake table tests results. Herein, the response quantity of interest is the maximum horizontal displacement of the center of mass (U) of the slab. While U is an output of the analytical model, the horizontal displacements (U) observed during the experimental campaign were calculated using the elongation/shortening measured by the four string potentiometers fixed to the slab. For this calculation, the slab was assumed as rigid body and the vertical displacements were neglected.

The analytical model does not account for sliding and twisting of the columns, or torsion of the slab, as it was observed in the experimental campaign. Thus, it is a very simple model—to the point of being simplistic, as it grossly overestimated the response of a rocking system in the PEER 2019 blind prediction contest (Vassiliou et al., 2021). With reference to Equations (4) and (5) and Fig. 3, the model parameters that were used are: $2R$ = 1.463m, α = 0.1359,$m_c g$ = 1.22 kN, $m_s g$ = 94.35 kN, and k_{res} = 1720 kN/m.

Fig. 5 presents the experimental and numerical Cumulative Distribution Functions (CDFs) of the maximum displacement of the slab's center of mass (U). The data is clustered in bins of different intensity (low- and high-intensity, as described in Section 3.3) and excitation types (NFP, NF, and FF, as described in Section 3.3). It also plots the 95% confidence interval (CI) of the experimentally obtained U. The model performs reasonably well, as it generally lies within the 95% CI.

To statistically validate the analytical model, a two-sample Kolmogorov-Smirnov test was conducted using the built-in Matlab routine "kstest2". This test rejects or accepts the null hypothesis (H_o) that both data are from the same distribution. The null hypothesis H_o is rejected when the p-value is lower than a given statistical significance value α_s. The p-value is a measure of the evidence against H_o and it does not represent the probability that H_o is true. In

this work, a fairly large value of statistical significance of 0.1 is used to allow for a nuanced qualification of null hypothesis validity using an evidence classification scale, shown in Table 1. Table 2 provides the *p*-values for all six sets shown in Fig. 5. The numerical CDF is compared to the experimental CDF of *U*. In 5/6 cases there is small to none evidence against both data coming from the same distribution, while in 1/6 there is medium–weak. Hence, this statistical test shows that the analytical model is a good predictor of the response of the center of mass of the slab.

Table 1. Evidence classification p-value scale

p-value	Evidence
<0.01	Very strong against H_o
0.01-0.05	Strong against H_o
0.05-0.10	Medium-weak against H_o
>0.10	Small or none against H_o

As *p*-values are not often used in earthquake engineering practice, Table 2 also presents the error of the median of *U*. In 5/6 cases, the error lies below 30%. In the high-intensity FF, the error is 47%—but the model is conservative. In no case did the model underestimate the median response by more than 30%. However, as the model disregards a number of physical mechanisms (e.g., energy dissipation, flexibility of the columns, geometric imperfections that lead to torsion), one cannot generalize, and more tests under more complicated and realistic geometries should be performed for its validation. Moreover, the model cannot predict the torsion of the slab and therefore it can only be used for the prediction of the center of the mass of the slab; not for the column drift ratios.

Table 2. Statistical comparison of the analytical model and the experimental data.

Set	*p*-value	$e_{50} = \frac{\lvert u_{50,\text{ana}} - u_{50,\text{exp}} \rvert}{u_{50,\text{exp}}}$
Low-intensity (NFP)	0.06	0.29
High-intensity (NFP)	0.86	0.02
Low-intensity (NF)	0.65	0.09
High-intensity (NF)	0.59	0.20
Low-intensity (FF)	0.26	0.09
High-intensity (FF)	0.15	0.47

4. Conclusions

This paper presents the statistical validation of a numerical model that predicts the response of a rigid-body rocking system. The experimental data used for the model validation was obtained from shaking table tests in a resilient system composed of four precast columns supporting a slab. The columns were only connected to the slab through ungrouted tendons in series with washer spring. The whole system was freely standing on top of the shaking table platform.

When statistically validating a model, it is not the response to individual ground motions that is of interest, but the statistics of the response to ensembles of ground motions. Therefore, this work compared the numerical and experimental CDF of the time maximum of the horizontal displacement of the center of mass of the slab. Using the two-sample Kolmogorov-Smirnov statistical test method, it was verified that the response probability distribution obtained numerically agrees reasonably well with response probability distribution observed experimentally. Furthermore, the median response of the numerical model and experimental tests were also compared, showing to be in good agreement. In no

case the numerical model underestimates the system's median response in more than 30%. Therefore, it can be concluded that, despite its simplicity, the numerical model was able to predict the statistics of the displacement of the center of mass of the slab to sets of ground motions that characterize the seismic hazard, namely the CDFs of the time maxima to individual excitations. The numerical model, however, cannot capture the experimentally observed torsion of the slab, and should be used carefully to predict the drift of the individual columns.

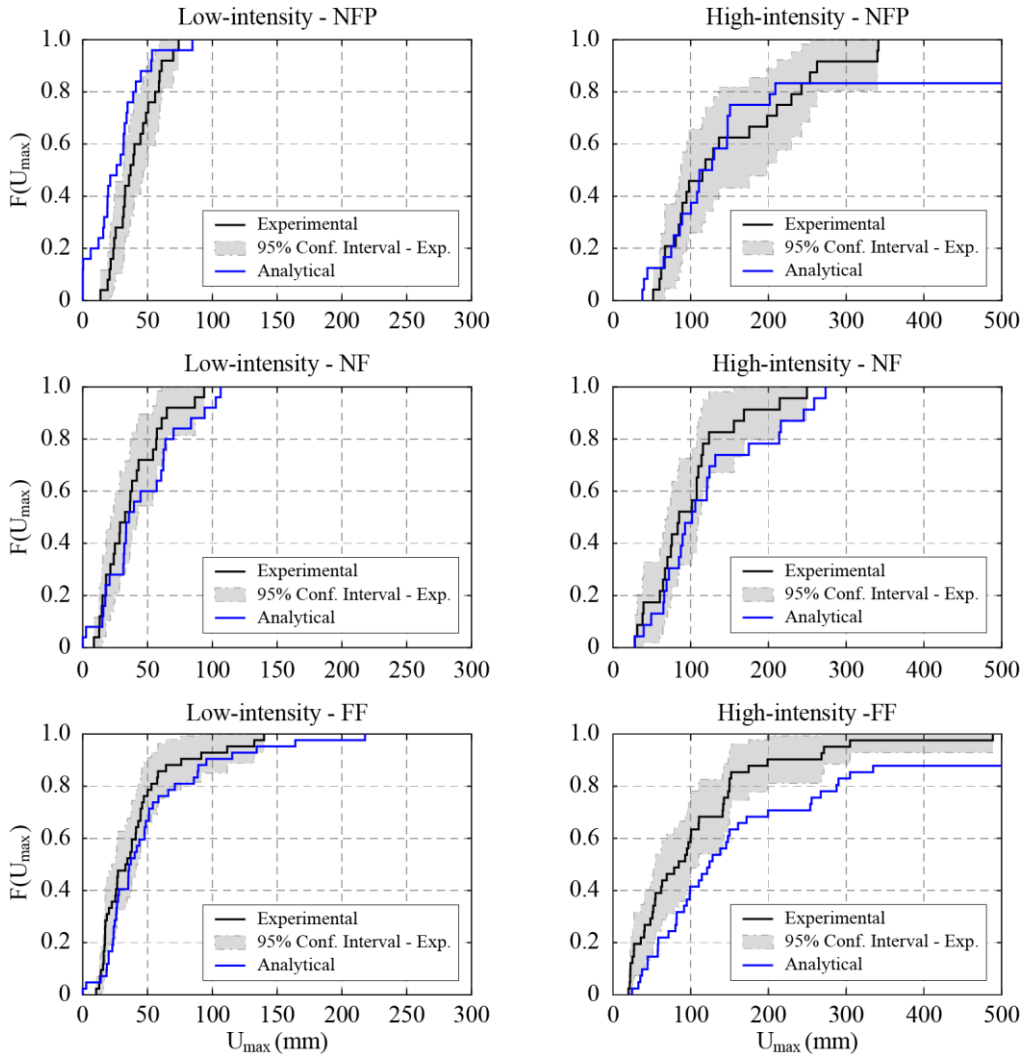

Fig. 5 – CDF plots obtained from the experimental data and CDF obtained using the analytical model.

Acknowledgements

This work was supported by the ETH Zurich under grant ETH-10 18-1. The authors would also like to acknowledge the support of EU funded project LightCoce, "Building an Ecosystem for the up-scaling of lightweight multi-functional concrete and ceramic materials and structures" (DT-NMBP-01-2018, www.lightcoce-oitb.eu), which provided access in concrete unit pilot line for the concrete production.

References

Bachmann JA, Strand M, Vassiliou MF, Broccardo M, Stojadinovic B (2018) Is rocking motion predictable?. Earthq Eng Struct Dyn. 47(2): 535-552.

Cohagen LS, Pang JBK, Stanton JF, Eberhard MO. (2008) A Precast Concrete Bridge Bent Designed to Re-Center after an Earthquake. Rep No. WA-RD 684.3/TNW 2008-09.

FEMA P695 (2009) Quantification of Building Seismic Performance Factors [Rep. FEMA P695]. Washington, D.C: Federal Emergency Management Agency.

Housner GW (1963) The behavior of inverted pendulum structures during earthquakes. Bull Seismol Soc Am. 53(2):403–417.

Kurama YC, Sritharan S, Fleischman RB, Restrepo JI, Henry RS, Cleland NM, Ghosh SK, Bonelli P (2018) Seismic-resistant precast concrete structures: state of the art. J. Struct. Eng. 144(4): 03118001.

Mashal, M. (2015). Post-tensioned earthquake damage resistant technologies for accelerated bridge construction., Doctoral Thesis, University of Canterbury

Makris N, Konstantinidis D (2003) The rocking spectrum and the limitations of practical design methodologies. Earthq Eng Struct Dyn. 32(2): 265–289.

Makris N, Vassiliou MF (2015) Dynamics of the rocking frame with vertical restrainers. J. Struct Eng. 141(10):04014245.

Mander, J. B., & Cheng, C. T. (1997). Seismic resistance of bridge piers based on damage avoidance design. In *Seismic resistance of bridge piers based on damage avoidance design* (pp. 109-109).

Palermo A, Pampanin S, Calvi GM. (2004) Use of 'Controlled Rocking' in the seismic design of Bridges. In proceedings of 13th World Conference on Earthquake Engineering 2004.

Qu H, Li T, Wang Z, Wei H, Shen J, Wang H. (2018) Investigation and verification on seismic behavior of precast concrete frame piers used in real bridge structures: Experimental and numerical study. Eng. Struct. 2018; 154: 1–9.

Reggiani Manzo N, Vassiliou MF (2022a) Cyclic tests of a precast restrained rocking system for sustainable and resilient seismic design of bridges. Engineering Structures 252: 113620.

Reggiani Manzo N, Vassiliou MF, Mouzakis H, Badogiannis E (2022b) Shaking table tests of a resilient bridge system with precast reinforced concrete columns equipped with springs. Earthq Eng Struct Dyn. 51(1): 213–239.

Reggiani Manzo N, Vassiliou MF, Mouzakis H, Badogiannis E, Karapitta L (2022c) Dataset from shaking table tests of a bridge system with precast reinforced concrete columns equipped with springs. ETH Research Collection Platform. DOI: 10.3929/ethz-b-000522686.

Salehi, M., Valigura, J., Sideris, P., & Liel, A. B. (2021). Experimental Assessment of Second-Generation Hybrid Sliding-Rocking Bridge Columns under Reversed Lateral Loading for Free and Fixed End Rotation Conditions. Journal of Bridge Engineering, 26(10), 04021071.

Sideris P, Aref AJ, Filiatrault A. (2015) Experimental Seismic Performance of a Hybrid Sliding–Rocking Bridge for Various Specimen Configurations and Seismic Loading Conditions. J. Bridg. Eng. 2015; 20(11): 04015009.

Thonstad, T., Mantawy, I. M., Stanton, J. F., Eberhard, M. O., & Sanders, D. H. (2016). Shaking table performance of a new bridge system with pretensioned rocking columns. J. Bridge Eng., *21*(4), 04015079.

Vassiliou MF (2018) Seismic response of a wobbling 3D frame. Earthq Eng Struct Dyn. 47(5):1212–1228.

Vassiliou MF, Broccardo M, Cengiz C, Dietz M, Dihoru L, Gunay S, Mosalam KM, Mylonakis G, Sextos A, Stojadinovic B (2021) Shake table testing of a rocking podium: results of a blind prediction contest. Earthq Eng Struct Dyn. 50(4): 1043–1062.

Vassiliou MF, Burger S, Egger M, Bachmann JA, Broccardo M, Stojadinovic B (2017) The three-dimensional behavior of inverted pendulum cylindrical structures during earthquakes. Earthq Eng Struct Dyn. 46(14): 2261–2280.

Vassiliou MF, Makris N (2015) Dynamics of the vertically restrained rocking column. J Eng Mech. 141(12):04015049.

Zhang Q, Shahria Alam M (2020) State-of-the-art of seismic-resistant precast bridge columns. J. Bridge Eng. 25(10): 03120001.